^{18}F-FDG Uptake in Reactive Neck Lymph Nodes of Oral Cancer: Relationship to Lymphoid Follicles

Tassei Nakagawa[1,2], Masatoshi Yamada[3], and Yoshio Suzuki[3]

[1]Department of Radiology, Asahi General Hospital, Chiba, Japan; [2]Department of Radiology, Faculty of Medicine, Asahi General Hospital, Tokyo Medical and Dental University, Tokyo, Japan; and [3]Department of Pathology, Asahi General Hospital, Chiba, Japan

PET using ^{18}F-FDG is acceptable as a preoperative diagnostic tool for head and neck cancer. PET combined with CT provides precise localization of neck lymph nodes. Reactive lymphadenopathy is well known as a principal cause of false-positive findings on PET/CT for nodal staging. We investigated the reactive lymph nodes of oral cancer to elucidate the ^{18}F-FDG–avid area in these nodes. **Methods:** Surgically dissected neck lymph nodes of oral cancer were retrospectively reviewed. Of the patients without pathologic nodal metastasis who underwent preoperative PET/CT, 11 patients with 31 enlarged lymph nodes at 20 levels were enrolled. The maximum standardized uptake value (SUVmax) of each lymph node was recorded. The diameters of the long and short axes were measured by pathologic sectioning, and the sectional surface area was calculated in square millimeters. Besides being stained with hematoxylin and eosin, the sections were immunohistochemically stained by CD79a for B cells, CD3 for T cells, CD68 for macrophages, CD21 for follicular dendritic cells (FDCs), and ubiquitous glucose transporter type 1 (GLUT1). The expression of GLUT1 was compared with staining of lymphoid cells. The numbers of total lymphoid follicles and hyperplastic secondary follicles were counted on CD21 and hematoxylin and eosin sections, respectively. The follicular reactivity index was determined as the ratio of secondary follicles relative to total follicles on the corresponding section. These parameters of reactive lymph nodes were analyzed on a level basis. **Results:** GLUT1 was expressed exclusively in lymphoid follicles, whose staining pattern was identical to that of FDCs. The calculated sectional area correlated significantly with the number of total follicles ($r = 0.560$; $P = 0.0101$). SUVmax did not correlate with the number of total follicles ($P = 0.8947$) but correlated significantly with the number of secondary follicles ($r = 0.535$; $P = 0.0152$). In addition, a strong positive correlation between SUVmax and the follicular reactivity index was demonstrated ($r = 0.829$; $P < 0.0001$). **Conclusion:** GLUT1 was expressed on cytoplasmic protrusions of FDCs in lymphoid follicles. The ^{18}F-FDG accumulation in reactive lymphadenopathy depended on secondary follicles. FDCs in germinal centers of secondary follicles are suggested to be avid for ^{18}F-FDG and the principal cause of false-positive findings for nodal staging.

Received Dec. 9, 2007; revision accepted Mar. 7, 2008.

For correspondence or reprints contact: Tassei Nakagawa, I-1326 Asahi-city, Chiba 289-2511, Japan.

E-mail: tnakagawa@hospital.asahi.chiba.jp

Key Words: follicular dendritic cell; germinal center; glucose transporter; reactive lymphadenopathy; oncology; PET/CT

J Nucl Med 2008; 49:1053–1059

DOI: 10.2967/jnumed.107.049718

PET is an imaging tool that provides biochemical and physiologic information (*1*). The glucose analog ^{18}F-FDG is transported into cells by facilitative glucose transporters (*2*). An overexpression of ubiquitous glucose transporter type 1 (GLUT1) in malignant tumors allows ^{18}F-FDG PET to have a useful role in oncology (*3*). The use of PET/CT for nodal staging is based on an increased ^{18}F-FDG accumulation in metastatic lymph nodes. In-line PET with CT, furthermore, enables precise localization of ^{18}F-FDG–avid spots on the conventional image and increases diagnostic accuracy for nodal staging in the head and neck (*4–6*). It is well known, however, that ^{18}F-FDG accumulates in areas of inflammation and in reactive lymphadenopathy (*7,8*). In previous articles, GLUT1 expression in lymphoid follicles was reported in mediastinal lymphadenopathy of lung cancer patients, which the authors concluded was a major cause of false-positive findings on PET/CT for nodal staging of lung cancer (*8,9*). The semiquantitative standardized uptake value (SUV) in lymph nodes, however, did not correlate with the area and grade of GLUT1 expression (*9*). Lymphoid follicles are composed of lymphocytes, macrophages, and follicular dendritic cells (FDCs). Networks of these cells in lymphoid follicles make up germinal centers, which can easily be seen on histologic sections stained with hematoxylin and eosin (H&E) (*10*) and can be differentiated by immunohistochemical methods; that is, B lymphocytes by CD79a (*11*), T lymphocytes by CD3 (*12*), macrophages by CD68 (*13*), and FDCs by CD21 (*14*).

The purpose of this study was to elucidate ^{18}F-FDG–avid cells in reactive lymphadenopathy. First, an immunohistochemical method was used on reactive neck lymphadenopathy of oral cancer to assess GLUT1 expression. Then, ^{18}F-FDG uptake in lymphadenopathy was evaluated by comparison with the lymphoid follicles.

MATERIALS AND METHODS

Patients

This retrospective research was approved by an institutional review board and did not require the informed consent of the patients. The cases of patients with oral cancer who underwent neck dissection with or without primary excision from March 2005 to May 2007 were reviewed. Twenty patients underwent PET/CT for clinically indicated nodal staging of newly diagnosed oral cancer and for the evaluation of clinically suspected recurrent lymphadenopathy in the neck. Patients with previous radiotherapy in the neck area or with pathologically proven neck metastases were excluded. With this exclusion, 14 patients with pathologically negative necks remained, and 11 patients (6 men and 5 women; average age, 62.6 y; range, 26–83 y) had lymphadenopathy at one or more levels. Thirty-one enlarged nodes exceeding 10 mm in maximal diameter (average, 13.5 mm; range, 10–19 mm) at 20 levels were included. PET/CT was performed within 1 mo before surgery (average, 21 d; range, 13–30 d). The pathologic finding for the enrolled patients was squamous cell carcinoma, except for 1 case of adenoid cystic carcinoma. The primary lesion was resected at this research in all patients except one, who had already undergone surgery for the primary excision. Two of the enrolled patients received oral chemotherapy before surgery. The other patients had no previous therapy for the neck lesion.

PET/CT

The patients received an intravenous injection of 3 MBq of ^{18}F-FDG per kilogram. The ^{18}F-FDG was produced in-house using a 10-MeV cyclotron (Cyclone 10/5; IBA) and an automated synthesis module (TRACERlab; GE Healthcare). All patients fasted for at least 6 h before tracer injection, and plasma glucose was in the acceptable range in all patients (mean, 84.8 mg/dL; range, 65–104 mg/dL). A PET/CT (Biograph LSO Duo; Siemens) study of the torso in arms-up position was started 110 min after the ^{18}F-FDG administration, took approximately 20 min, and was followed by imaging of the head and neck with the patient's arms down. Thus, a tracer uptake period of 130 min was allowed for the dedicated head and neck scan. The CT (2-detector system) data were used for attenuation correction of the PET emission images.

The CT parameters of the dedicated head and neck scan were as follows: 3-mm slice width; 2.5-mm collimation; 1.5-s gantry rotation; 5-mm gantry feed per rotation; 130-kVp tube voltage; 67-mA tube current; and 500-mm field of view. PET emission data were acquired in 3-dimensional mode with a spatial resolution of 6 mm in full width at half maximum. The dedicated head and neck PET parameters were as follows: 2 bed positions at 3 min per position; 162-mm axial field of view; and 585-mm transaxial field of view. The reconstruction zoom factor was 2, and the reconstructed images had 1.3-mm pixels displayed in a 256×256 matrix.

Lymph Node Matching and Image Analyses

All patients underwent unilateral or bilateral neck dissection, and the surgeon assigned each lymph node to a neck level. The excised nodes were fixed in formalin, embedded in paraffin, sectioned, and stained with H&E separately for each neck level. Of the patients with a pathologically negative neck, enlarged lymph nodes exceeding 10 mm on the section were included in the study. The maximum diameters in the long and short axes were measured on the section. Then, size was calculated as the sectional area in square millimeters, approximately by the formula for an oval area; that is, 0.8× (the product of a long- and a short-axis diameter).

The included lymph nodes were identified on the CT image (*15*). Because it was difficult to discriminate each node if more than one node was enlarged at the same level, the average value in that level was used in such cases. A workstation featuring PET and CT fusion (e.soft; Siemens) was used for image display and analysis. An oval region of interest was placed on the largest displayed lymph node. The SUV of the pixels in that region of interest was calculated using the formula $SUV = C_{tis}/(dose/wt)$, where C_{tis} is the decay-corrected tracer tissue concentration (Bq/mL), assuming a tissue density of 1 g/mL; dose is the injected total dose (Bq); and wt is the patient's body weight (g). The maximum SUV (SUVmax) in the region of interest was recorded as a semiquantitative evaluation of ^{18}F-FDG uptake in the lymph nodes.

Immunohistochemistry

Immunohistochemistry by the biotin–avidin immunoenzymatic method was performed on the included lymph nodes. Sections 4 μm thick were freed of paraffin (using xylene) and rehydrated in a graded ethanol series. Tissue antigens were retrieved by microwave irradiation (CD79α, CD68) or by autoclaving (GLUT1, CD3, and CD21; 121°C for 15 min) with a 10 mmol/L concentration of citrate buffer (pH 6.0). An automated staining machine (Autostainer; DAKO) was used, and the sections were rinsed with phosphate-buffered saline (pH 7.6) between each step. After endogenous peroxidase blocking by 3% hydrogen peroxide, the sections were incubated with primary antibodies: rabbit anti-GLUT1 polyclonal

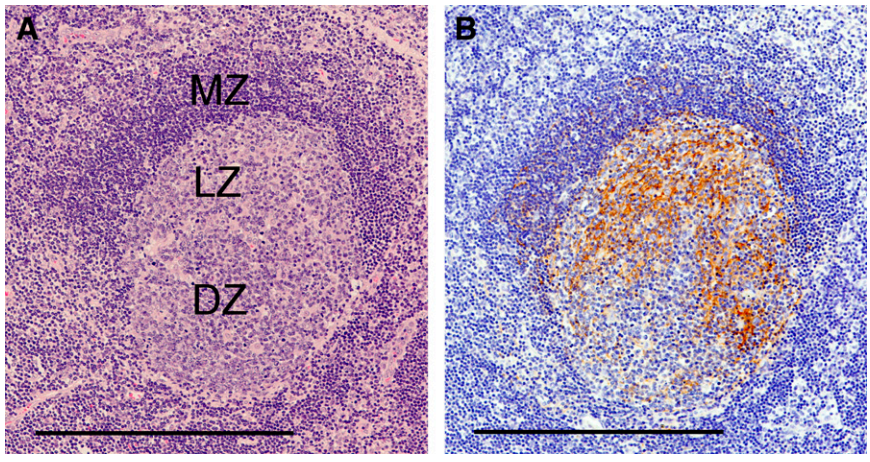

FIGURE 1. Secondary lymphoid follicle in neck node (in left level II of patient 7). (A) Hyperplastic germinal center composed of light zone (LZ) and dark zone (DZ) is asymmetrically surrounded by darkly stained mantle zone (MZ) (H&E; bar, 250 μm). (B) On CD21 section, fingerprintlike configuration formed by protrusions of FDCs is characteristically depicted, notably in light zone (bar, 250 μm; ×100).

TABLE 1
Patients and Reactive Neck Lymph Nodes

Patient no.	Age (y)	Sex	Primary site	T stage	Pathology	Interval* (d)	Previous therapy	Level of LNs	Diameter of LNs (mm)	SUVmax of LNs	No. of total follicles	No. of secondary follicles	Follicular reactivity index (%)
1	58	F	R tongue	T1	SCC	13		L II†	12.5 × 7.5	2.10‡	120	37.5	31.3
2	63	F	L buccal mucosa	T2	SCC	23	Operation§	R II†	11.5 × 5.5	2.91	82	21.5	26.2
3	55	M	R tongue	T1	SCC	17		R II†	15 × 10.5	2.58	92.5	30	32.4
								R III	19 × 8	1.34	67	3	4.5
4	78	M	Palate	T1	Adenoid cystic carcinoma	28		R II†	14 × 7.5	1.83	147	6	4.1
								L II†	14 × 8	2.08	115.5	13	11.3
5	63	M	R tongue	T1	SCC	28	Chemotherapy‖	R II¶	12 × 9	3.73	70.3	29.8	42.3
6	72	F	R buccal mucosa	T1	SCC	21	Chemotherapy‖	R II†	10 × 8	2.05	61.5	5.5	8.9
								R III†	10 × 8	1.85	95	4	4.2
7	64	M	L tongue	T1	SCC	16		L II	16 × 10	2.17	198	46	23.2
8	68	F	R tongue	T1	SCC	15		R II	15 × 8	1.90	66	9	13.6
9	59	M	L gingiva	T1	SCC	30		L II	19 × 8	1.43	66	4	6.1
10	26	M	R tongue	T2	SCC	23		L I	12 × 7	1.47	98	20	20.4
								R II	14 × 10	1.82	128	13	10.2
								L II	12 × 7	2.91	57	20	35.1
								R III	14 × 9	3.22	115	41	35.7
								L III	16 × 10	2.75	162	55	34.0
								R V†	13.5 × 8.5	2.35	90	25.5	28.3
11	83	F	R gingiva	T2	SCC	27		R I	10 × 7	2.28	73	21	28.8
								R II	18 × 11	2.15	188	49	26.1

*Days between PET/CT study and surgery.
†Average values of 2 lymph nodes.
‡SUV was estimated on PET image of torso.
§Primary lesion and ipsilateral neck LNs had been resected 1 y and 8 mo before.
‖Chemotherapy by tegafur with gimeracil (TS-1; Taiho) had been taken orally for 1 mo before operation.
¶Average values of 4 lymph nodes.
Level I = submental and submandibular nodes; level II = upper deep cervical nodes; level III = middle deep cervical nodes; level IV = lower deep cervical nodes; level V = spinal accessory and transverse cervical nodes.
SCC = squamous cell carcinoma; LNs = lymph nodes.

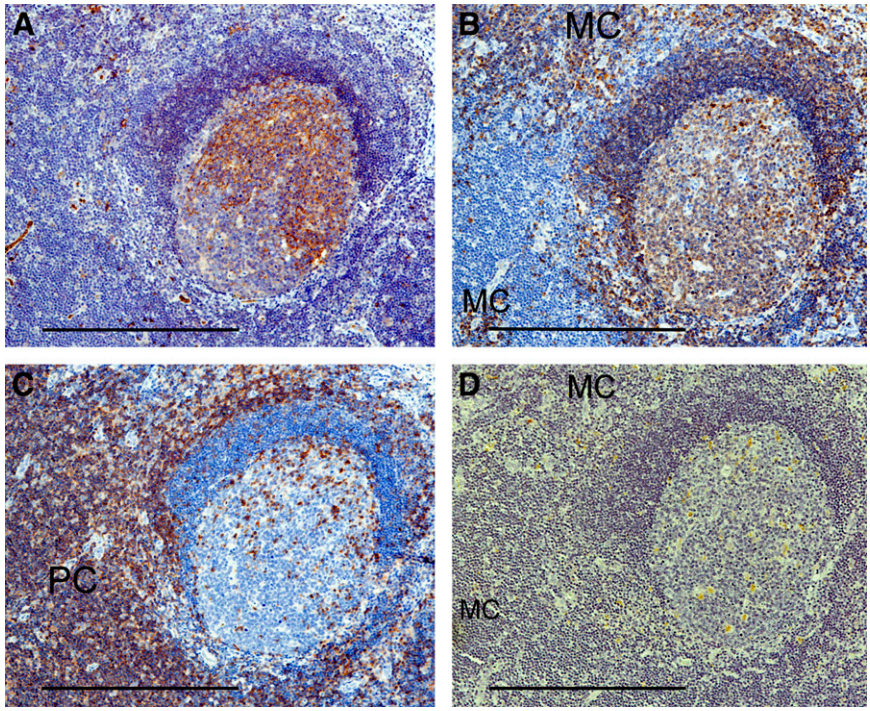

FIGURE 2. Secondary follicle stained by GLUT1 (A), CD79a (B), CD3 (C), and CD68 (D) (same follicle as in Fig. 1). (A) Marked similarity of staining pattern between GLUT1 and CD21 (Fig. 1B) in germinal center is noted. Erythrocytes seen in extrafollicular area are positive controls. (B) B cells are numerous in lymphoid follicle and medullary cords (MC). (C) T cells predominate in paracortex (PC), and a few are also seen within germinal center. (D) Macrophages are dispersed in germinal center and medullary cord (MC) and are rarely seen in paracortex (bar, 250 μm; ×100).

antibody (1:100; DAKO), anti-CD79α (1:60, clone JCB 117; DAKO), anti-CD3 (clone PS1; Nichirei), anti-CD68 (1:60, clone KP1; DAKO), and anti-CD21 (1:60, clone 1F8; DAKO). The sections then were incubated with biotinylated secondary antibody and peroxidase-labeled streptavidin–biotin complex (LSAB kit; DAKO). Finally, the sections were treated with diaminobenzidine as chromogen and counterstained with hematoxylin.

Lymphoid Follicles

Functionally, there are 2 types of lymphoid follicles. Secondary lymphoid follicles are considered functionally reactive to antigenic stimuli and are characterized by a germinal center and a surrounding asymmetric mantle zone. Primary follicles, in contrast, are typically small, with or without a symmetric concentric mantle zone. Lymphoid follicles containing FDCs are explicitly demonstrated on CD21 sections even if the follicles are too small to be recognized on H&E sections. On H&E sections, in contrast, the mantle zone surrounding the germinal center is easily recognized as a darkly staining area.

At first, the total follicles on the section were counted by CD21 staining. Secondary follicles were counted on the corresponding H&E section. Because secondary follicles are not necessarily seen completely on histologic sections, we chose as the area to be counted either a germinal center exceeding 0.25 mm in diameter with or without a mantle zone or a germinal center surrounded by a mantle zone with an asymmetric concentric configuration regardless of its sectional size (Fig. 1). The follicular reactivity index was then determined as the ratio of secondary follicles relative to total follicles in the section.

Statistical Analysis

The correlation between the nodal SUVmax and other nodal parameters was determined using the Pearson correlation coefficient. A P value of less than 0.05 was considered statistically significant.

RESULTS

SUVmax in Reactive Lymph Nodes

The included lymph nodes are summarized in Table 1. When more than one lymph node was present at the same level, the average values for SUVmax, diameter, number of follicles, and follicular reactivity index were used for the analyses for that level. For lymphadenopathy with an SUVmax ranging from 1.34 to 4.53 (average, 2.24), 3 nodes on 2 levels were false-positive, with a cutoff of 3.5. SUVmax was not associated with nodal size calculated as area in square millimeters ($P = 0.5281$).

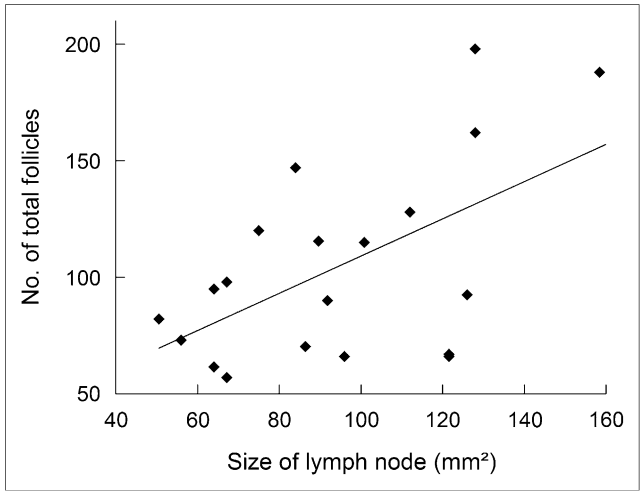

FIGURE 3. Nodal size calculated as cut surface area in square millimeters shows positive correlation with number of total lymphoid follicles. Solid line indicates linear best fit.

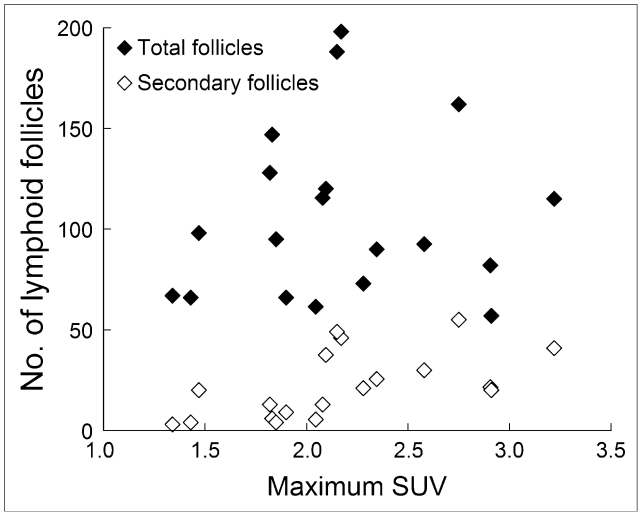

FIGURE 4. No relationship is seen between number of total lymphoid follicles and SUVmax of lymph nodes. In contrast, SUVmax shows positive relationship with number of secondary follicles.

GLUT1 Expression in Lymphoid Follicles

Immunohistochemistry demonstrated that GLUT1 was expressed in lymphoid follicles other than the erythrocytes of positive controls in the extrafollicular area. The immunohistochemistry for lymphoid cells showed a distribution different from that of GLUT1, with the exception of CD21. The staining pattern in lymphoid follicles for GLUT1 was markedly similar to that for CD21, which was characterized by a fingerprintlike configuration (Fig. 2A). In secondary follicles, GLUT1 staining was relatively localized to the germinal center whereas CD21 staining was beyond the germinal center. In addition, the cortical side of the germinal center was predominantly stained by both GLUT1 and CD21, with areas of variation. B cells, on CD79a sections, were observed in cortical areas, including lymphoid follicles and the medullary cord (Fig. 2B). T cells, on CD3 sections, were observed mainly in the paracortex and scattered in the germinal centers of secondary follicles (Fig. 2C). Macrophages, on CD68 sections, were observed in the medullary cords to a variable degree and dispersed within lymphoid follicles (Fig. 2D).

^{18}F-FDG Uptake and Follicular Reactivity

The number of total lymphoid follicles counted on CD21 sections correlated significantly with nodal size ($r = 0.560$; $P = 0.0101$) (Fig. 3). No relationship between nodal SUVmax and the number of total lymphoid follicles was noted ($P = 0.8947$) (Fig. 4). However, nodal SUVmax correlated significantly with the number of secondary follicles ($r = 0.535$; $P = 0.0152$) (Fig. 5A). In addition, the follicular reactivity index, ranging from 1.9% to 57.5% (average, 21.4%) on a nodal basis, showed a strong positive correlation with SUVmax on a level basis ($r = 0.829$; $P < 0.0001$) (Fig. 5B).

DISCUSSION

In the routine clinical setting, we perform PET/CT with a tracer uptake period of 110 min for whole-body imaging and 130 min for head and neck imaging. We apply an uptake period longer than the standard because of previous reports about the usefulness of delayed PET imaging for detecting malignant lesions, including nodal metastases (*16–18*). In nodal staging, however, there is a trade-off of some false-positive findings against the false-negatives. The sensitivity and specificity for neck nodal staging in our study were 75.0% and 94.4%, respectively, on whole-body imaging with a cutoff SUV of 3.5. With the same cutoff value, sensitivity and specificity on dedicated head and neck imaging were 75.0% and 89.5%, respectively. This assessment, whose values are in line with other articles (*5,19,20*), was performed for lymphadenopathy that could be detected on CT and calculated on a level basis. Compared with whole-body imaging, dedicated head and neck scanning showed an increase in SUVmax for most lymph nodes. There were reactive nodes, even a few with an SUVmax exceeding the cutoff value, only in head and neck imaging. Furthermore, as other investigators reported (*21–23*), there were occult metastatic nodes showing an SUVmax of much less than the cutoff value. Thus, it is not surprising that the dedicated head and neck imaging had a higher false-positive rate (10.5%) than the whole-body scanning (5.6%) without having an improved sensitivity. In addition, false-positive nodes are likely to be due to constant stimuli by carcinogenic and extrinsic antigens.

The current study showed that GLUT1 was expressed exclusively in lymphoid follicles, as has been found by

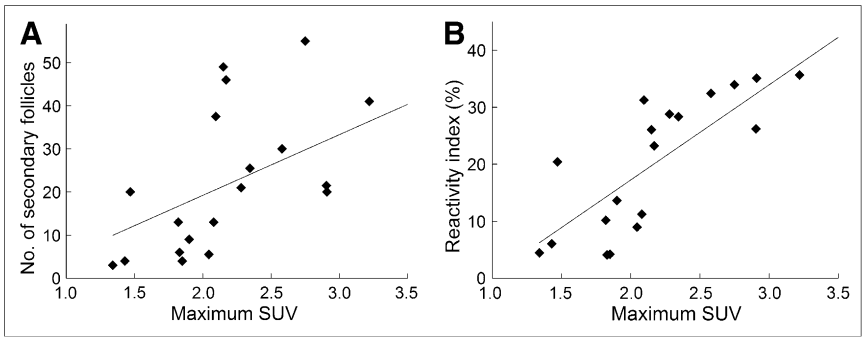

FIGURE 5. (A) Maximum SUV of lymph nodes correlates significantly with number of secondary follicles. (B) Strong positive correlation is seen between SUVmax of lymph nodes and follicular reactivity index. Solid lines indicate linear best fit.

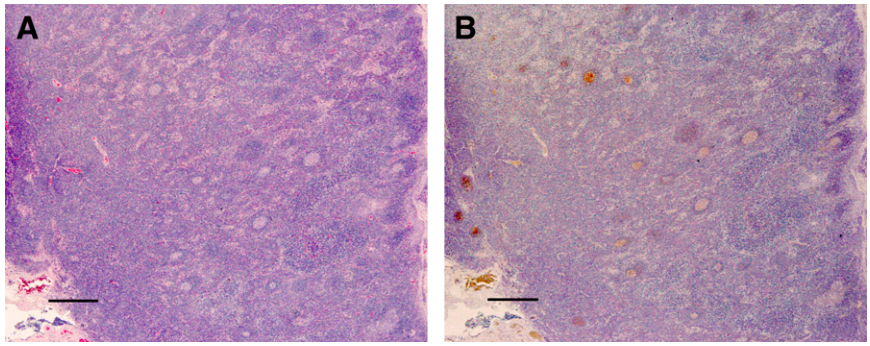

FIGURE 6. Lymphadenopathy of neck. (A) Enlarged lymph node with true-negative ^{18}F-FDG uptake (in right level III of patient 3) shows enlargement in extrafollicular area on H&E section. (B) Small primary follicles dispersed in lymph node are recognized on CD21 section (bar, 500 μm; ×20).

other investigators (*8,9*). The identical staining pattern found between GLUT1 and CD21 suggests that FDCs in lymphoid follicles express GLUT1 but does not indicate, however, that ^{18}F-FDG accumulates in all lymphoid follicles harboring FDCs, because the number of total follicles was not associated with nodal SUVmax. Rather, a significant correlation between secondary follicles and nodal SUVmax increases the likelihood that ^{18}F-FDG accumulates in secondary follicles.

Immunohistochemistry by lymphoid cells reflects the functions of lymph nodes, which comprise cortex, paracortex, medullary cord, and lymph-filled sinus. Lymphadenopathy is recognized when any of these components become enlarged. B cells predominate in the cortex, where lymphoid follicles generally exist, and plasma cells of B cell linkage predominate in the medullary cords. T cells predominate in the paracortex and are partially seen in the lymphoid follicles. Macrophages with phagocytized debris typically remain in the sinus or medullary cord, and some macrophages (tangible body macrophages) are dispersed in the germinal center. Primary follicles housing B cells are stimulated to secondary follicles when they encounter an antigenic presentation in which the germinal center is formed in association with other lymphoid cells (*24*). T cells also encounter an antigen displayed on dendritic cells in the paracortex, and the migration of T cells to lymphoid follicles is essential to germinal center formation (*25,26*). Secondary follicles with germinal centers involute when this follicular-center cell reaction is over (*27*), resulting in the deposit of memory cells and macrophages in the extrafollicular area. Local immunologic reactions, thus, remain in the extrafollicular area after secondary follicles involute, contributing to extrafollicular enlargement (Fig. 6). Secondary follicles are sometimes found deep in lymph nodes, especially with increased ^{18}F-FDG accumulation (Fig. 7). Therefore, both small primary and hyperplastic secondary follicles contribute to nodal enlargement, explaining the significant correlation between nodal size and the number of total follicles.

In the germinal centers of secondary follicles, B cell maturation from centroblasts to plasma cell precursors takes place through processes such as proliferation, differentiation, and apoptosis. This follicular-center cell reaction occurs in association with T cells, macrophages, and FDCs. Centroblasts on the deep side of follicles (dark zone) evolve to centrocytes on the cortical side (light zone), where they undergo somatic hypermutation to make antigen receptors that perfectly fit the presented antigen. The polarity of the germinal center shown by GLUT1, FDC, and T cells explains that centrocytes were near the FDC network in association with T cells during this trial-and-error process (*25,28,29*). ^{18}F-FDG appears to accumulate in FDCs within germinal centers, where FDCs play an important role in B cell maturation.

In the present study, the SUVmax of reactive lymph nodes ranged up to 4.53, and the highest follicular reactivity index of 57.4% was found at the same level. It was uncertain, however, if both highest values were estimated in the same node and if the follicular reactivity index could be extrapolated to a higher value on a nodal basis. Moreover, this study was performed solely on oral cancer patients. Further investigations need to be performed on larger sample sizes and in other regional lymphadenopathies. We believe, however, that

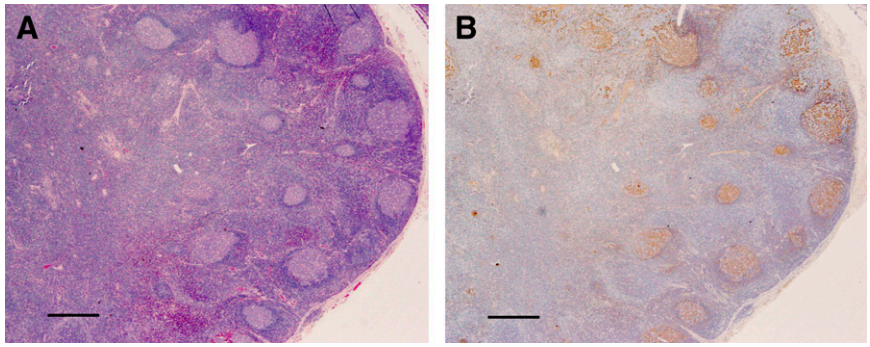

FIGURE 7. Reactive lymphadenopathy of neck. (A) Enlarged lymph node with false-positive ^{18}F-FDG uptake (in right level II of patient 5) shows hyperplastic lymphoid follicles on H&E section. (B) Hyperplastic germinal centers located in deeper area and in cortex are demonstrated on CD21 section (bar, 500 μm; ×20).

FDCs express glucose transporter in lymphoid follicles even if they are located in other regions and are avid for glucose when they are functionally active.

To our knowledge, this is the first report of FDCs producing false-positive findings on ^{18}F-FDG PET for nodal staging. Germinal centers harboring FDCs and other lymphoid cells are physiologically found in the extralymphoid organs, such as in the gastrointestinal tract. FDCs probably have an important role when the organs react to local antigenic stimuli in concert with the lymphoid cells. Despite much research about ^{18}F-FDG uptake in various inflammatory processes, GLUT1 expression in FDCs never has been recognized. Therefore, the present finding should be helpful in understanding the accumulation of ^{18}F-FDG in inflammatory processes and its physiologic mechanism.

CONCLUSION

The current study suggests that FDCs located in lymphoid follicles express GLUT1. ^{18}F-FDG uptake in reactive lymph nodes is associated with secondary follicles. Therefore, FDCs in the germinal centers of secondary follicles may be avid for ^{18}F-FDG.

ACKNOWLEDGMENTS

We thank Tetsuya Uno for excellent technical assistance. We also thank Isao Umehara, Katsuya Yoshida, Masakazu Akiba, Yuji Murata, and Hitoshi Shibuya.

REFERENCES

1. Rohren EM, Turkington TG, Coleman RE. Clinical applications of PET in oncology. *Radiology.* 2004;231:305–332.
2. Mueckler M. Facilitative glucose transporters. *Eur J Biochem.* 1994;219:713–725.
3. Smith TA. Facilitative glucose transporter expression in human cancer tissue. *Br J Biomed Sci.* 1999;56:285–292.
4. Adams S, Baum RP, Stuckensen T, Bitter K, Hor G. Prospective comparison of ^{18}F-FDG PET with conventional imaging modalities (CT, MRI, US) in lymph node staging of head and neck cancer. *Eur J Nucl Med.* 1998;25:1255–1260.
5. Schöder H, Yeung HW, Gonen M, et al. Head and neck cancer: clinical usefulness and accuracy of PET/CT image fusion. *Radiology.* 2004;231:65–72.
6. Jeong HS, Baek CH, Son YI, et al. Use of integrated ^{18}F-FDG PET/CT to improve the accuracy of initial cervical nodal evaluation in patients with head and neck squamous cell carcinoma. *Head Neck.* 2007;29:203–210.
7. Kubota R, Yamada S, Kubota K, et al. Intratumoral distribution of fluorine-18-fluorodeoxyglucose in vivo: high accumulation in macrophages and granulation tissues studied by microautoradiography. *J Nucl Med.* 1992;33:1972–1980.
8. Chung JH, Cho KJ, Lee SS, et al. Overexpression of glut1 in lymphoid follicles correlates with false-positive ^{18}F-FDG PET results in lung cancer staging. *J Nucl Med.* 2004;45:999–1003.
9. Chung JH, Lee WW, Park SY, et al. FDG uptake and glucose transporter type 1 expression in lymph nodes of non-small cell lung cancer. *Eur J Surg Oncol.* 2006;32:989–995.
10. von der Walk P, Meijer CJLM. Lymph nodes. In: Mills SE, ed. *Histology for Pathologists.* 3rd ed. Philadelphia, PA: Lippincott Williams & Wilkins; 2007: 763–780.
11. Mason DY, Cordell JL, Brown MH, et al. CD79a: a novel marker for B-cell neoplasms in routinely processed tissue samples. *Blood.* 1995;86:1453–1459.
12. Steward M, Bishop R, Piggott NH, et al. Production and characterization of a new monoclonal antibody effective in recognizing the CD3 T-cell associated antigen in formalin-fixed embedded tissue. *Histopathology.* 1997;30:16–22.
13. Pulford KA, Rigney EM, Micklem KJ, et al. KP1: a new monoclonal antibody that detects a monocyte/macrophage associated antigen in routinely processed tissue sections. *J Clin Pathol.* 1989;42:414–421.
14. Maeda K, Matsuda M, Suzuki H, et al. Immunohistochemical recognition of human follicular dendritic cell (FDCs) in routinely processed paraffin sections. *J Histochem Cytochem.* 2002;50:1475–1485.
15. Som PM, Curtin HD, Mancuson AA. Imaging-based nodal classification for evaluation of neck metastatic adenopathy. *AJR.* 2000;174:837–845.
16. Hustinx R, Smith RJ, Benard F, et al. Dual time point fluorine-18 fluorodeoxyglucose positron emission tomography: a potential method to differentiate malignancy from inflammation and normal tissue in the head and neck. *Eur J Nucl Med.* 1999;26:1345–1348.
17. Zhuang H, Pourdehnad M, Lambright ES, et al. Dual time point ^{18}F-FDG PET imaging for differentiating malignant from inflammatory processes. *J Nucl Med.* 2001;42:1412–1417.
18. Ma SY, See LC, Lai CH, et al. Delayed ^{18}F-FDG PET for detection of paraaortic lymph node metastases in cervical cancer patients. *J Nucl Med.* 2003;44:1775–1783.
19. Vermeersch H, Loose D, Ham H, et al. Nuclear medicine imaging for the assessment of primary and recurrent head and neck carcinoma using routinely available tracers. *Eur J Nucl Med Mol Imaging.* 2003;30:1689–1700.
20. Schöder H, Yeung HW. Positron emission imaging of head and neck cancer, including thyroid carcinoma. *Semin Nucl Med.* 2004;34:180–197.
21. Stoeckli SJ, Steinert H, Pfaltz M, et al. Is there a role for positron emission tomography ^{18}F-fluorodeoxyglucose in the initial staging of nodal negative oral and oropharyngeal squamous cell carcinoma. *Head Neck.* 2002;24:345–349.
22. Schöder H, Carlson DL, Kraus DH, et al. ^{18}F-FDG PET/CT for detecting nodal metastases in patients with oral cancer staged N0 by clinical examination and CT/MRI. *J Nucl Med.* 2006;47:755–762.
23. Nahmias C, Carlson ER, Duncan LD, et al. Positron emission tomography/computerized tomography (PET/CT) scanning for preoperative staging of patients with oral/head and neck cancer. *J Oral Maxillofac Surg.* 2007;65:2524–2535.
24. Allen CD, Okada T, Cyster JG. Germinal-center organization and cellular dynamics. *Immunity.* 2007;27:190–202.
25. Garside P, Ingulli E, Merica RR, et al. Visualization of specific B and T lymphocyte interactions in the lymph node. *Science.* 1998;281:96–99.
26. Cyster JG, Ansel KM, Reif K, et al. Follicular stromal cells and lymphocyte homing to follicles. *Immunol Rev.* 2000;176:181–193.
27. Vinuesa CG, Cook MC. The molecular basis of lymphoid architecture and B cell responses: implications for immunodeficiency and immunopathology. *Curr Mol Med.* 2001;1:689–725.
28. Li L, Choi YS. Follicular dendritic cell-signaling molecules required for proliferation and differentiation of GC-B cells. *Semin Immunol.* 2002;14:259–266.
29. Kosco-Vilbois MH. Are follicular dendritic cells really good for nothing? *Nat Rev Immunol.* 2003;3:764–769.